Extensional troughs in the Caloris Basin of Mercury: Evidence of lateral crustal flow

Thomas R. Watters Center for Earth and Planetary Studies, National Air and Space Museum, Smithsonian Institution, Washington, DC 20560-0315, USA
Francis Nimmo Department of Earth Sciences, University of California–Santa Cruz, Santa Cruz, California 95064, USA
Mark S. Robinson Center for Planetary Sciences, Northwestern University, Evanston, Illinois 60208, USA

ABSTRACT

Thirty years ago Mariner 10 revealed extensional troughs that form giant polygons in the floor material of the Caloris impact basin, Mercury. The polygonal troughs occur in the interior of the basin and overprint wrinkle ridges formed in an earlier stage of compression. In contrast, lunar and martian basins exhibit extensional troughs that are circumferential and confined to basin margins. Loading by basin-filling material can explain the extensional and compressional features seen in deformed lunar and martian basins, but not the existence of the Caloris polygonal troughs. Here we suggest that the Caloris troughs formed from late-stage basin uplift and extension due to lateral flow of a relatively thick crust toward the basin center. If such lateral flow occurs, the resulting timing, location, and magnitude of the extensional stresses predicted by our model are consistent with those inferred from the polygonal troughs. These results are not strongly dependent on the degree of lateral flow or the assumed crustal rigidity. For a dry plagioclase rheology and likely radiogenic heat fluxes, the crustal thickness around Caloris is 90–140 km. Similar late-stage uplift and extension probably do not occur in basins on the Moon and Mars because their crusts are too thin to allow analogous lateral flow.

Keywords: Mercury, Caloris Basin, tectonics, uplift, crustal flow.

INTRODUCTION

The Caloris Basin has a main rim diameter estimated to be 1300 km (Strom et al., 1975), making it one of the largest impact basins in the solar system. While less than half of the basin was imaged by Mariner 10 (1974–1975), the imaged portion is characterized by localized smooth plains. These plains are extensively deformed by basin-concentric and basin-radial compressional wrinkle ridges (Fig. 1A), a pattern common in lunar mare basins (Strom, 1972; Bryan, 1973; Maxwell et al., 1975). The wrinkle ridges likely formed in response to compression that resulted from subsidence of the interior fill material (see Melosh and McKinnon, 1988). Recent mapping of lobate scarp thrust faults in exterior smooth plains and intercrater plains indicates that they formed at roughly the same time as the basin-interior wrinkle ridges (Watters et al., 2004). This timing suggests that the formation of the wrinkle ridges was aided by a compressional stress bias in the lithosphere, possibly due to global contraction. The most remarkable landforms in the Caloris Basin are complex extensional troughs (Strom et al., 1975; Dzurisin, 1978) that crosscut the wrinkle ridges and are thus among the youngest endogenic features in the basin. In plan view, the troughs are highly variable, consisting of linear and sinuous segments (Fig. 1B) that range in width from hundreds of meters up to ~10 km (Dzurisin, 1978). In the wider troughs where the interiors are not obscured by shadows, the floors appear to be flat, consistent with the interpretation that the troughs are graben (Strom et al., 1975; Dzurisin, 1978). The troughs, like the wrinkle ridges, are both basin concentric and basin radial, forming giant polygons (Strom et al., 1975; Dzurisin, 1978; Melosh and Dzurisin, 1978) as much as 40–50 km across (Watters et al., 2005). The distribution of orientations indicates that troughs are predominantly basin concentric (Pechmann, 1980). Although polygonal troughs remarkably similar in morphology and scale to those in Caloris have been found in the northern lowlands of Mars (Carr et al., 1976; Pechmann, 1980; McGill, 1986) and in volcanic plains on Venus (Johnson and Sandwell, 1992; Smrekar et al., 2002), no analogous landforms occur in the floor materials of impact basins on the Moon or Mars.

CALORIS POLYGONAL TROUGHS

Our topographic profiles (based on photoclinometry) confirm that at least some of the Caloris troughs have relatively flat floors (Fig. 2). The walls of the troughs have gentle slopes, generally 4° to 6° (not exceeding 10°), and depths vary from ~100 m up to a maximum of ~220 m ($n = 7$). Topographic profiles indicate that many troughs are flanked on both sides by gently sloping rises (Fig. 2) and that trough rims are often offset relative to each other, some by as much as tens of meters. Martian polygonal troughs also exhibit flanking rises (Hiesinger and Head, 2000) and offset rims.

The extensional troughs in Caloris do not occur uniformly across the basin floor. They are distributed in a broad arc that extends from ~180 km to ~450 km inward from the basin rim (Fig. 1A). It is not known if troughs extend beyond ~450 km toward the basin center into the unimaged hemisphere. However, the location of the most prominent polygonal troughs suggests that the peak extensional strains occurred ~180–450 km from the basin rim.

The displacement/length (D/L) ratio γ and the dips of the trough-forming normal faults can be used to estimate the extensional strain

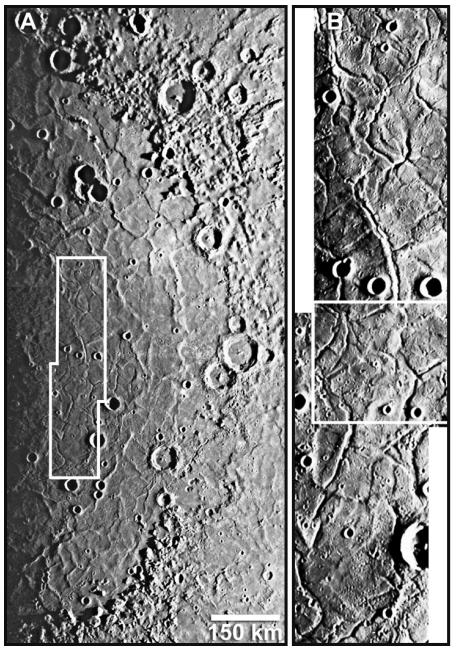

Figure 1. Polygonal troughs in Caloris Basin, Mercury. A: Interior plains of Caloris Basin show evidence of compressional (wrinkle ridges) and extensional (troughs) deformation (Mariner 10 image mosaic is centered near 32°N, 180°W). B: High-resolution image mosaic of a portion of interior plains showing extensional troughs that form giant polygons. Area is shown by white box in A (Mariner 10 images 0529055 and 0529056). Maximum width of mosaic is ~115 km.

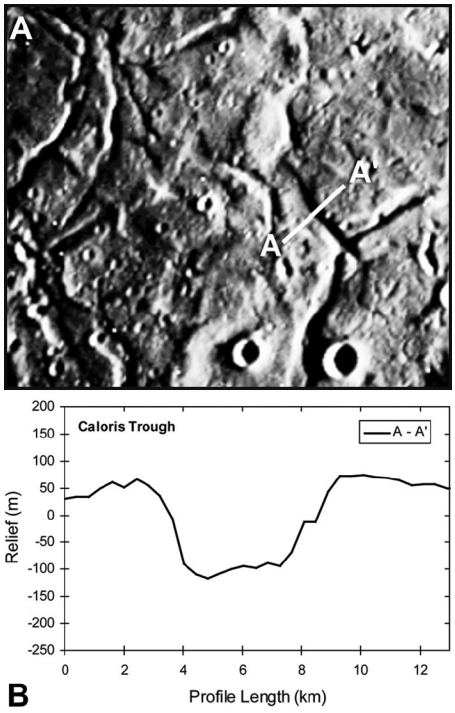

Figure 2. Topography of Caloris troughs. A: Prominent troughs make up the largest polygons on the imaged portion of the floor of Caloris (sub-frame of Mariner 10 image 0529056 shown by white box in Fig. 1B). B: Topographic profile shows the trough has relatively flat floor, gently sloping walls, and raised or rounded rims (profile location is shown in A). The topographic profile was generated using two-dimensional photoclinometry (Kirk et al., 2003) on Mariner 10 image 0529055. Elevations are relative to an arbitrary datum (vertical exaggeration ~20:1).

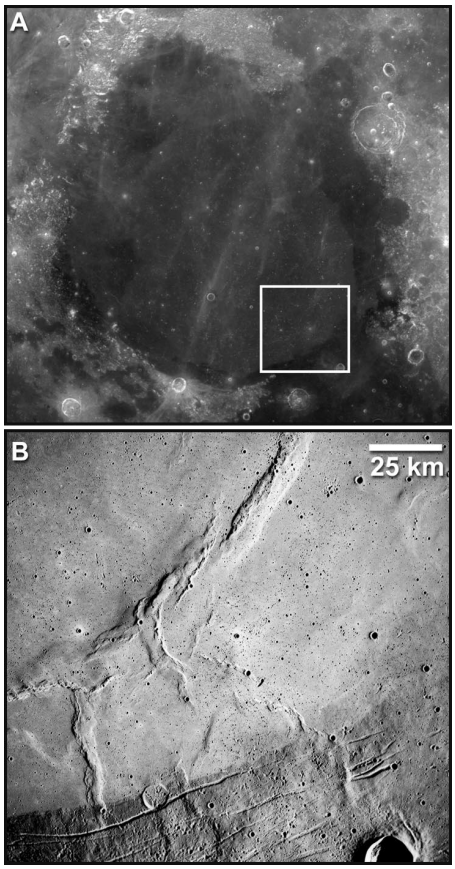

Figure 3. Mare Serenitatis on the Moon. A: Serenitatis is a lunar impact basin ~600 km in diameter that was filled by mare basalts, resulting in a mass concentration or mascon (Clementine 750 nm image mosaic). B: Basin-concentric and basin-radial wrinkle ridges occur in interior, and circumferential troughs formed by arcuate graben are confined to basin margin (Apollo 17 Metric Camera image AS17-0452). Area is shown by white box in A.

expressed by the polygonal troughs (Scholz and Cowie, 1990; Cowie et al., 1993). The shallow slopes of the trough walls are very similar to measured slopes of martian polygonal troughs (Hiesinger and Head, 2000). Such slopes are much lower than likely fault-plane dips on bounding normal faults (>45°). The shallow trough wall slopes are possibly due to mass wasting related to impact processes that have, over time, reduced slopes below the angle of repose. Estimates of the displacement on the normal faults range from 0.11 to 0.25 km with an average of ~0.2 km ($n = 7$), assuming initial fault-plane dips characteristic of normal faults (~60°). The value of γ obtained by a linear fit to the D/L data for the troughs is $\sim 2.2 \times 10^{-3}$ ($\theta = 60°$). The estimate of γ is complicated by the variability of the trough widths, and the linkage relationship between fault segments is not obvious. Assuming that each trough segment is independent, our estimate of the extensional strain over the total area of the imaged portion of the Caloris Basin is ~0.05%. For a Young's Modulus of 100 GPa, this strain corresponds to an elastic stress of ~50 MPa.

COMPARISON WITH MASCON BASINS

The basin-interior extensional troughs of Caloris distinguish it from other deformed impact basins. Deformed basins on the Moon and Mars are characterized by radial and concentric wrinkle ridges in the interior fill and circumferential trough-forming graben at the basin margins (Fig. 3). Lunar graben form arcuate or linear troughs with flat floors and steep walls (Baldwin, 1963; McGill, 1971; Golombek, 1979), occur in parallel or en echelon sets, and can cut both mare and basin material (Wilhelms, 1987). This pattern of deformation is the signature of mascon (mass concentration) tectonics, where loading from uncompensated fill material results in downward flexure of the lithosphere, giving rise to compressional stresses in the interior of the basin that form wrinkle ridges, and extensional stresses on the margins that form circumferential graben (Phillips et al., 1972; Melosh, 1978; Solomon and Head, 1979, 1980; Freed et al., 2001). By contrast, in the Caloris Basin the extensional polygons are found toward the basin center and crosscut the wrinkle ridges, indicating that the polygons postdate the ridges (Strom et al., 1975; Dzurisin, 1978; Melosh and McKinnon, 1988). Deformation of the floor material in Caloris progressed from a period of compression to a later period of extension.

Melosh and McKinnon (1988) proposed a model for the origin of the basin-interior extensional stresses that involves exterior annular loading from the emplacement of exterior smooth plains adjacent to Caloris. In their model, the annular load causes basin-interior extension, which results in concentric normal faults for a range of lithospheric thickness of 75–125 km (Melosh and McKinnon, 1988). Critical to this model is the timing of emplacement of the basin-exterior smooth plains that create the annular load. The emplacement of Caloris interior fill material and the compression that formed the wrinkle ridges must predate the emplacement of exterior smooth plains.

LATERAL CRUSTAL FLOW MODEL

Here we propose a new model for the origin of the extensional troughs that can account for both the location and timing of their formation, independent of the basin-exterior smooth plains. Our model is based on the lateral flow of subsurface crustal material into the Caloris Basin. Evidence suggests that the basin was partially filled with smooth plains volcanic material shortly after it formed (Spudis and Guest, 1988). We assume that the subsidence and compression that formed the wrinkle ridges was contemporaneous with the emplacement of the basin-filling smooth plains, as is the case in lunar maria (cf. Watters, 1988). The crust beneath the basin, however, was probably still thinner than the surrounding crust. This lateral crustal thickness contrast gives rise to lateral pressure gradients, which can drive flow toward the basin center even if the basin is isostatically compensated (Nimmo and Stevenson, 2001). Lateral crustal flow will result in late-stage uplift of the existing basin materials (Fig. 4A) at a rate determined by the crustal thickness, rheology, and thermal gradient. The rate of flow is always slower than the vertical mantle response to surface loading (Zhong, 1997), but can still be significant. If lateral flow does occur, the result is uplift by an amount dependent on the initial thinning of the crust and the lithospheric rigidity; such uplift results in extension. Although the long-wavelength topography of Caloris is only poorly constrained, the basin appears to be relatively shallow (e.g., Schaber et al., 1977), consistent within the occurence of uplift.

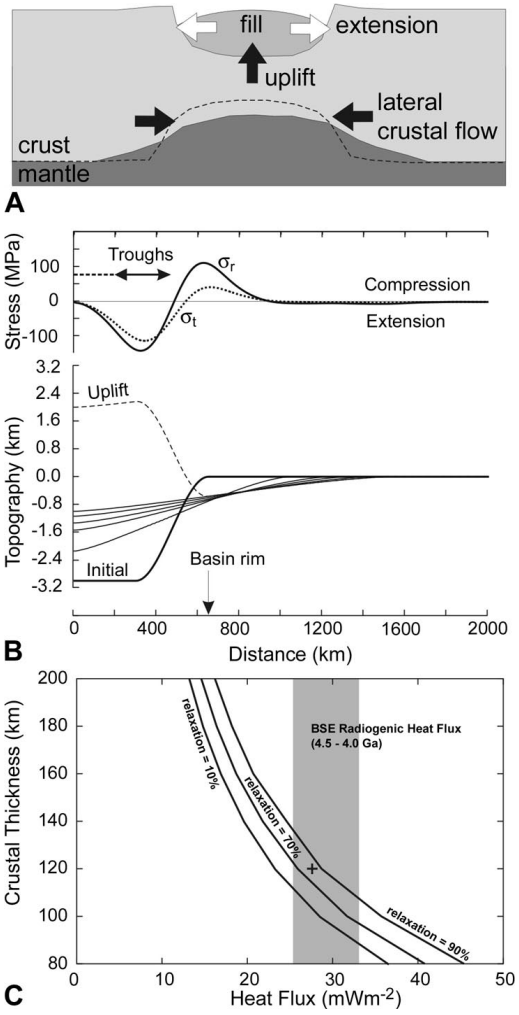

Figure 4. Lateral crustal flow model (see text). A: Schematic of effect of lateral crustal flow on basin topography. Initial base of crust is indicated by dotted line; lateral flow causes uplift at center and extension. B: Model of lower crustal flow, using method of Nimmo and Stevenson (2001) with dry plagioclase rheology. Lower panel: Bold line outlines pan-shaped initial isostatically compensated basin topography; thin lines detail evolution of topography at 24, 94, 174, 334, and 500 m.y.; dashed line shows total (isostatic) uplift. Model assumes constant mantle heat flux of 23.7 mWm^{-2} and crustal thickness of 120 km; other parameters were given by Nimmo and Watters (2004). Upper panel shows stresses caused by uplift, assuming an elastic thickness of 50 km and Young's Modulus of 100 GPa. Radial stresses are denoted by σ_r, tangential stresses by σ_t. Location of polygonal troughs imaged in Caloris denoted by horizontal arrow; dashed line (upper panel) denotes poorly or unimaged area. C: Degree of basin relaxation (ratio of initial basin depth to central uplift) as a function of heat flux and crustal thickness after 500 m.y. Shaded region denotes radiogenic heat flux on Mercury assuming bulk silicate earth (BSE) concentrations; cross denotes model shown in B.

In order to estimate the amount of uplift and the corresponding stresses, the evolution of the topography of a Caloris-sized impact basin was simulated over a 500 m.y. period (Fig. 4B). The evolution of an isostatically compensated crust of varying thickness $H(x)$ is given by

$$\frac{dH}{dt} = -\frac{d}{dx}K\left|\frac{\partial H}{\partial x}\right|^{n-1}\frac{\partial H}{\partial x}, \quad (1)$$

where n is the exponent in the stress-strain relationship, t is time, and K is an effective diffusivity, which depends on the vertically varying viscosity of the crust (see Nimmo and Stevenson, 2001, for further details). The resulting contrast between the initial and final crustal thickness $\Delta H(x)$ may then be calculated. This change in crustal thickness generates a load, which results in surface displacement and stresses. The deflection w caused by the load is calculated using the approach of Comer et al. (1985):

$$w(k) = \frac{\Delta H(k)(\rho_m - \rho_c)}{\rho_m + Dk^4/g}. \quad (2)$$

Here k is the wavenumber (for an axisymmetric geometry), ρ_m and ρ_c are the mantle and crustal densities, respectively, g is the acceleration due to gravity, and D is the flexural rigidity given by $D = ET_e^3/12(1 - \nu^2)$, where E is Young's Modulus, T_e is the elastic thickness, and ν is Poisson's ratio. Note that in the limit of zero rigidity, equation 2 results in the usual isostatic equation, as required. Given the deflection $w(k)$, the surface stresses may be calculated using the approach outlined in Comer et al. (1985, their Appendix B), taking the elastic limit. There is an inconsistency arising from the fact that the lower crustal flow (equation 1) assumes isostasy ($T_e = 0$), while calculating the stresses requires a finite elastic thickness. However, in the cases considered in this paper, where the flexural wavelength is much shorter than the wavelength over which flow occurs, the errors introduced by this approach are very small. Note also that a flat-plate geometry is assumed; the use of a spherical shell geometry (e.g., Freed et al., 2001) is unlikely to generate significantly different results.

The initial basin shape is flat floored, in agreement with recent studies of gravity anomalies associated with lunar mascons (Watters and Konopliv, 2001). The lower-crustal flow model (Nimmo and Stevenson, 2001) was used to calculate the evolution of the basin topography, assuming a temperature- and stress-dependent dry plagioclase rheology, a crustal thickness (120 km), and heat flux (23.7 mWm^{-2}) consistent with previous estimates (Anderson et al., 1996; Nimmo and Watters, 2004). Lateral flow occurs in a channel at the base of the crust where the (vertically varying) viscosity is lowest; the rate of flow decreases with time due to the reduction in driving stresses. The redistribution of crustal material generates an upward load, which causes progressively slowing uplift and stresses (Fig. 4B).

For the assumed initial basin geometry, the surface radial and tangential extensional stresses reach a peak value of ~100 MPa ~300 km inwards of the basin rim (Fig. 4B). The elastic thickness assumed here (50 km) results in a flexural parameter much smaller than the basin width; thus, the assumption of isostasy for the lower-crustal flow calculations is justified. The predicted location and the magnitude of the stresses from lateral crustal flow are compatible with the observations of the Caloris polygonal troughs. This result suggests that lateral crustal flow is the cause of the observed graben.

Crustal flow can occur for a wide range of crustal thicknesses, rheologies, and heat flows (see following). Neither the location nor the magnitude of the peak extensional stresses is significantly affected as the degree of basin relaxation (ratio of initial to final basin central depth) varies from 10% to 80%. As long as the flexural parameter α remains small compared to the basin width, variations in α affect the magnitude but not the location of the peak stresses. Similar stress magnitudes are obtained for an initially Gaussian basin shape; however, in this case peak extension is predicted at the basin center.

Partial basin relaxation is the main requirement to generate the stress patterns shown in Figure 4B. The degree of relaxation depends on the crustal thickness, rheology, and heat flux (Nimmo and Stevenson, 2001). The degree of relaxation as a function of heat flux and crustal thickness for the assumed dry plagioclase rheology is shown in Figure 4C. The inferred crustal thickness is in the range of 90–140 km, assuming the heat flux on Mercury is due to radiogenic elements present in the same concentrations as the bulk silicate Earth. This range in thickness is compatible with previous estimates of 100–300 km (Anderson et al., 1996; Nimmo and Watters, 2004). Different rheologies would generate

different inferred crustal thicknesses, but we emphasize that the stress pattern shown in Figure 4B only requires moderate lateral flow to have occurred and is not dependent on a specific rheology. The crustal thickness can be further constrained with topography and gravity data to be returned early next decade by the recently launched MESSENGER mission (Solomon et al., 2001).

The absence of extensional troughs in the floor material of impact basins on the Moon and Mars suggests different conditions on Mercury. Ancient heat fluxes on the Moon were probably comparable to those on Mercury, but the lunar crust is only 60 km thick on average (Neumann et al., 1996); the crustal thickness around Orientale, comparable in size and age to Caloris, is estimated to be no more than ~80 km (Neumann et al., 1996). Figure 4C shows that, under these conditions, lateral flow is unlikely to have occurred. Heat fluxes were probably larger for Mars than Mercury, but martian crustal thicknesses are generally smaller than lunar values, so basin uplift on Mars may have been rare. Furthermore, subsequent volcanism and sedimentation are likely to have buried any such martian features. Thus, the circumstances that produced the polygonal troughs in the Caloris Basin and allowed them to survive (i.e., a relatively thick crust and lack of subsequent geologic activity) may be unique to Mercury.

ACKNOWLEDGMENTS

We are grateful for the thoughtful reviews of Jay Melosh and William B. McKinnon. This material is based upon work supported by the National Aeronautics and Space Administration under grants issued through the Office of the Planetary Geology and Geophysics Program.

REFERENCES CITED

Anderson, J.D., Jurgens, R.F., Lau, E.L., and Slade, M.A., 1996, Shape and orientation of Mercury from radar ranging data: Icarus, v. 124, p. 690–697, doi: 10.1006/icar.1996.0242.

Baldwin, R.B., 1963, The measure of the Moon: Chicago, University of Chicago Press, 488 p.

Bryan, W.B., 1973, Wrinkle-ridges as deformed surface crust on ponded mare lava: Geochimica et Cosmochimica Acta, supplement 1, p. 93–106.

Carr, M.H., Masursky, H., Baum, W.A., Blasius, K.R., Briggs, G.A., Cutts, J.A., Greeley, R., Guest, J.E., Soderblom, L.A., Smith, B.A., Veverka, J., and Wellman, J.B., 1976, Preliminary results form the Viking orbiter imaging experiment: Science, v. 193, p. 766–776.

Comer, R.P., Solomon, S.C., and Head, J.W., 1985, Mars: Thickness of the lithosphere from the tectonic response to volcanic loads: Reviews of Geophysics, v. 23, p. 61–92.

Cowie, P.A., Scholz, C.H., Edwards, M., and Malinverno, A., 1993, Fault strain and seismic coupling on mid-ocean ridges: Journal of Geophysical Research, v. 98, p. 17,911–17,920.

Dzurisin, D., 1978, The tectonic and volcanic history of Mercury as inferred from studies of scarps, ridges, troughs, and other lineaments: Journal of Geophysical Research, v. 83, p. 4883–4906.

Freed, A.M., Melosh, H.J., and Solomon, S.C., 2001, Tectonics of mascon loading: Resolution of the strike-slip faulting paradox: Journal of Geophysical Research, v. 106, p. 20,603–20,620, doi: 10.1029/2000JE001347.

Golombek, M.P., 1979, Structural analysis of lunar grabens and the shallow crustal structure of the Moon: Journal of Geophysical Research, v. 84, p. 4657–4666.

Hiesinger, H., and Head, J.W., 2000, Characteristics and origin of polygonal terrain in southern Utopia Planitia, Mars: Results from Mars orbiter laser altimeter and Mars Orbiter camera data: Journal of Geophysical Research, v. 105, p. 11,999–12,022, doi: 10.1029/1999JE001193.

Johnson, C.L., and Sandwell, D.T., 1992, Joints in Venusian lava flows: Journal of Geophysical Research, v. 97, p. 13,601–13,610.

Kirk, R.L., Barrett, J.M., and Soderblom, L.A., 2003, Photoclinometry made simple. . . ? [abs.], *in* Advances in planetary mapping 2003: Houston, International Society for Photogrammetry and Remote Sensing, http://wwwflag.wr.usgs.gov/USGSFlag/Space/Isprs/MEETINGS/Houston2003/abstracts/.

Maxwell, T.A., El-Baz, F., and Ward, S.W., 1975, Distribution, morphology, and origin of ridges and arches in Mare Serenitatis: Geological Society of America Bulletin, v. 86, p. 1273–1278, doi: 10.1130/0016-7606(1975)862.0.CO;2.

McGill, G.E., 1971, Attitude of fractures bounding straight and arcuate lunar rilles: Icarus, v. 14, p. 53–58, doi: 10.1016/0019-1035(71)90101-1.

McGill, G.E., 1986, The giant polygons of Utopia, northern Martian plains: Geophysical Research Letters, v. 13, p. 705–708.

Melosh, H.J., 1978, The tectonics of mascon loading: Proceedings of the 9th Lunar and Planetary Science Conference, Houston: Geochimica et Cosmochimica Acta, v. 3, supplement 10, p. 3513–3525.

Melosh, H.J., and Dzurisin, D., 1978, Tectonic implications for gravity structure of Caloris Basin, Mercury: Icarus, v. 33, p. 141–144, doi: 10.1016/0019-1035(78)90029-5.

Melosh, H.J., and McKinnon, W.B., 1988, The tectonics of Mercury, *in* Vilas, F., et al., eds., Mercury: Tucson, University of Arizona Press, p. 374–400.

Neumann, G.A., Zuber, M.T., Smith, D.E., and Lemoine, F.G., 1996, The lunar crust: Global structure and signature of major basins: Journal of Geophysical Research, v. 101, p. 16,841–16,864, doi: 10.1029/96JE01246.

Nimmo, F., and Stevenson, D.J., 2001, Estimates of Martian crustal thickness from viscous relaxation of topography: Journal of Geophysical Research, v. 106, p. 5085–5098, doi: 10.1029/2000JE001331.

Nimmo, F., and Watters, T.R., 2004, Depth of faulting on Mercury: Implications for heat flux and crustal and effective elastic thickness: Geophysical Research Letters, v. 31, p. L02701, doi: 10.1029/2003GL018847.

Pechmann, J.C., 1980, The origin of polygonal troughs on the northern plains of Mars: Icarus, v. 42, p. 185–210, doi: 10.1016/0019-1035(80)90071-8.

Phillips, R.J., Conel, J.E., Abbott, E.A., Sjogren, W.L., and Morton, J.B., 1972, Mascons: Progress toward a unique solution for mass distribution: Journal of Geophysical Research, v. 77, p. 7106–7114.

Schaber, G.G., Boyce, J.M., and Trask, N.J., 1977, Moon-Mercury large impact structures, isostasy and average crustal viscosity: Physics of the Earth and Planetary Interiors, v. 15, p. 189–201, doi: 10.1016/0031-9201(77)90031-0.

Scholz, C.H., and Cowie, P.A., 1990, Determination of geologic strain from fault slip data: Nature, v. 346, p. 837–839, doi: 10.1038/346837a0.

Smrekar, S.E., Moreels, P., and Franklin, B.J., 2002, Characterization and formation of polygonal fractures on Venus: Journal of Geophysical Research, v. 107, p. 5098, doi: 10.1029/2001JE001808.

Solomon, S.C., and Head, J.W., 1979, Vertical movement in mare basins relation to mare emplacement, basin tectonics and lunar thermal history: Journal of Geophysical Research, v. 84, p. 1667–1682.

Solomon, S.C., and Head, J.W., 1980, Lunar mascon basins: Lava filling, tectonics, and evolution of the lithosphere: Reviews of Geophysics and Space Physics, v. 18, p. 107–141.

Solomon, S.C., McNutt, R.L., Jr., Gold, R.E., Acuña, M.H., Baker, D.N., Boynton, W.V., Chapman, C.R., Cheng, A.F., Gloeckler, G., Head, J.W., III, Krimigis, S.M., McClintock, W.E., Murchie, S.L., Peale, S.J., Phillips, R.J., Robinson, M.S., Slavin, J.A., Smith, D.E., Strom, R.G., Trombka, J.I., and Zuber, M.T., 2001, The MESSENGER mission to Mercury: Scientific objectives and implementation: Planetary and Space Science, v. 49, p. 1445–1465, doi: 10.1016/S0032-0633(01)00085-X.

Spudis, P.D., and Guest, J.E., 1988, Stratigraphy and geologic history of Mercury, *in* Vitas, F., et al., eds., Mercury: Tucson, University of Arizona Press, p. 118–164.

Strom, R.G., 1972, Lunar mare ridges, rings and volcanic ring complexes: Modern Geology, v. 2, p. 133–157.

Strom, R.G., Trask, N.J., and Guest, J.E., 1975, Tectonism and volcanism on Mercury: Journal of Geophysical Research, v. 80, p. 2478–2507.

Watters, T.R., 1988, Wrinkle ridge assemblages on the terrestrial planets: Journal of Geophysical Research, v. 93, p. 10,236–10,254.

Watters, T.R., and Konopliv, A.S., 2001, The topography and gravity of Mare Serenitatis: Implications for subsidence of the mare surface: Planetary and Space Science, v. 49, p. 743–748, doi: 10.1016/S0032-0633(01)00007-1.

Watters, T.R., Robinson, M.S., Bina, C.R., and Spudis, P.D., 2004, Thrust faults and the global contraction Mercury: Geophysical Research Letters, v. 31, p. L04701, doi: 10.1029/2003GL019171.

Watters, T.R., Nimmo, F., and Robinson, M.S., 2005, The origin of polygonal troughs in the Caloris Basin of Mercury [abs.], *in* Proceedings, Lunar and Planetary Science Conference, 36th: Houston, Lunar and Planetary Institute, # 1449.

Wilhelms, D.E., 1987, The geologic history of the Moon: Washington, D.C., U.S. Government Printing Office, 302 p.

Zhong, S., 1997, Dynamics of crustal compensation and its influences on crustal isostasy: Journal of Geophysical Research, v. 102, p. 15,287–15,299, doi: 10.1029/97JB00956.

Manuscript received 3 March 2005
Revised manuscript received 30 March 2005
Manuscript accepted 1 April 2005

Printed in USA